NDT&E International 45 (2012) 16–21

Contents lists available at SciVerse ScienceDirect

NDT&E International

journal homepage: www.elsevier.com/locate/ndteint

Non-destructive measurements of large case depths in hardened steels using the thermal-wave radar

R. Velazquez-Hernandez [a,b], A. Melnikov [b], A. Mandelis [b,*], K. Sivagurunathan [b], M.E. Rodriguez-Garcia [c], J. Garcia [b]

[a] División de Investigación y Posgrado, Facultad de Ingeniería, Universidad Autónoma de Querétaro, Cerro de las Campanas S/N, C.P. 76010, Querétaro, Qro., México
[b] Center for Advanced Diffusion-Wave Technologies, Department of Mechanical and Industrial Engineering, University of Toronto, ON, Canada M5S 3G8
[c] Departamento de Nanotecnología, Centro de Física Aplicada y Tecnología Avanzada, Universidad Nacional Autónoma de México, Campus Juriquilla, Querétaro, Qro., México

ARTICLE INFO

Article history:
Received 19 March 2011
Received in revised form
16 August 2011
Accepted 20 August 2011
Available online 3 September 2011

Keywords:
Thermal-wave radar
Hardness
Case depth
Steels
NDT

ABSTRACT

The thermal-wave radar method was used to resolve and measure deep hardness case depths (2–3 mm) of AISI9310 and Pyrowear53 steels used in the aerospace industry. Several gears made of these steels were evaluated and correlations between radiometric signal and case depths were obtained using the cross-correlation peak delay time. The foregoing case depth range is significantly deeper than achievable with point-by-point laser frequency scans (800 μm) and swept-sine modulation of the laser beam (1.16 mm).

1. Introduction

Reliable hardness and case depth measurements are very important for the quality control of case-hardened steels and the assessment of the effectiveness of heat treating processes. The current industrial technique to make these measurements uses a mechanical indenter and is destructive and time consuming. Many non-destructive methodologies such as electromagnetic, ultrasound, and photothermal have been reported to obtain these parameters [1–7]. For example, with regard to hardened steel depths, an ultrasonic signal processing technique using deconvolution by Wiener filtering followed by autoregressive spectral extrapolation [4] significantly improves the separation of echoes from the top surface and the transition zone between the hardened layer and the soft core and has improved the capability of ultrasonic measurements to resolve depths <2 mm. Among them photothermal techniques have shown strong potential and advantages over other evaluation methods due to the ability of thermal waves to monitor subsurface structures and damage in (usually opaque) manufacturing materials well beyond the optical penetration depth. The thermal diffusivity, which depends on the microstructural properties of a material, is very sensitive to the changes that take place in the material as a result of surface modification processes such as case hardening. Considering this change in thermal diffusivity at case depths commensurate with typical thermal-wave penetration lengths (a few hundred micrometers up to $\sim$1 mm), photothermal techniques have proven to be excellent nondestructive and noncontact methods for depth profiling subsurface inhomogeneities [8,9]. This depth profiling capability has been applied to the evaluation of discretely layered structures in composite or inhomogeneous materials through thermal diffusion length probing by scanning the modulation frequency of the incident laser power [10,11].

Recently, applications of photothermal radiometry (PTR) to the measurement of the effective case depth in case-hardened industrial steels have been reported [11,12,13]. However, the reported case depths are less than 1 mm due to the loss of depth resolution in the low-frequency range below 1 Hz. To overcome the depth resolution limitation of conventional thermal waves, a laser-intensity modulation chirped PTR method has been introduced and named "Thermal Wave Radar" (TWR) [14]. Owing to photothermal signal generation and detection methods adapted from radar science, this technique is able to detect subsurface inhomogeneities well beyond the effective thermal–diffusion–length-limited range of conventional PTR. In this thermal-wave modality the matched filter compression signal processing method well-known from the ultrasonic radar technology [15] is employed to increase the signal-to-noise ratio (SNR). In matched filtering, the role of chirped modulation is to compress the energy delivered by the chirp into a narrow correlation peak, which enables imaging with maximum SNR and axial resolution. The result is a reduction in the width of the cross-correlation (CC) main lobe (peak) and an

* Corresponding author.
E-mail address: mandelis@mie.utoronto.ca (A. Mandelis).

0963-8695/$ - see front matter © 2011 Elsevier Ltd. All rights reserved.
doi:10.1016/j.ndteint.2011.08.006

increase in the amplitude of the peak, as the area below it represents the total energy imparted into the system/target. In the case of a linear frequency sweep, the SNR gain factor of the ideal matched filter is equal to the time-bandwidth product of the chirp. Theoretical and experimental studies, which also depict TWR optical excitation and thermal-wave response waveforms, have shown that this increase in SNR also holds in the photothermal field [14]. The high SNR and the chirp frequency spectrum compression into one CC peak are the reasons of enhanced depth resolution beyond the thermal–diffusion–length limit of conventional frequency-domain PTR. The closest photothermal technique to TWR is the pseudo random binary sequence (PRBS) modulation [16,17]. Comparison shows that the main advantage of the earliest version of TWR (frequency modulated time-delay domain technique [16,18]) over PRBS is its superior dynamic range, which leads to enhanced SNR.

The purpose of this work is to extend the depth resolution of photothermal methods to the measurement of deep hardness case depths using the TWR. Specifically the peak delay time of the PTR cross-correlation function is studied as a function of case depth in two types of industrial steel samples used in the aerospace sector, AISI9310 and Pyrowear53. These steels exhibited depth profilometric saturation of case hardened depths beyond 1 mm in our previous studies [13] where frequency swept sine-wave laser beam modulation was used. Those earlier studies allow a direct comparison with the TWR method.

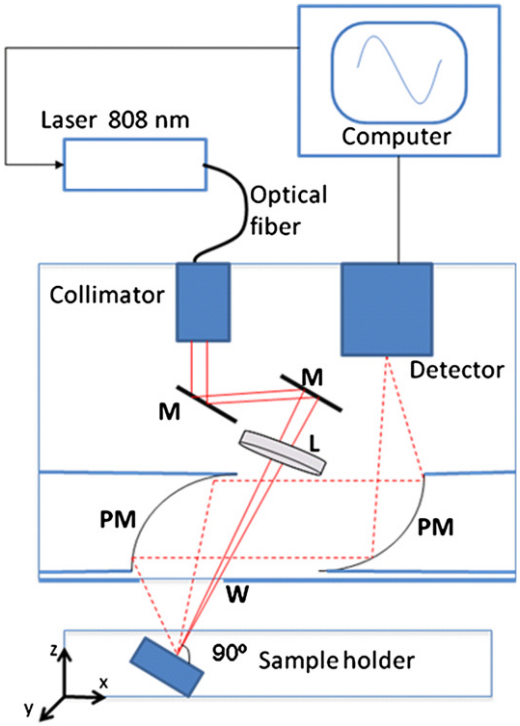

Fig. 1. Schematic diagram of the PTR TWR system. *M*1 and *M*2 are steered mirrors; *L*, lens; *PM*1 and *PM*2, paraboloidal mirrors; *W*, CaF_2 window.

2. Experimental setup

A schematic diagram of the PTR TWR instrument developed specifically for the purpose of on-line measurements of small industrial steel parts is shown in Fig. 1. The source of thermal-wave excitation was a 808 nm diode-laser (dc output 4.5 W, model VDM00018, JENOPTIK, Germany). The laser output was modulated by a periodic current driver. Waveform and frequency content were controlled by a computer equipped with a data acquisition card (NI-PCI-4461, National Instruments, USA). The modulated laser beam was fiber-coupled into a collimator. The collimated output was steered to a lens (*L*) by mirrors (*M*1, *M*2) and then focused onto the sample. To facilitate the focusing process the sample was placed in an automated sample holder with 3 Cartesian degrees of freedom (x–y–z motion). Spatially resolved imaging may be achieved through point-by-point scanning of the laser beam on the sample surface by moving the sample. The samples were positioned perpendicular to the laser beam. The mid-IR signal generated in response to laser power absorption and optical-to-thermal energy conversion in the form of blackbody emission was collected by a parabolic mirror (*PM*1) through the CaF_2 window (*W*) (99% transmission for both excitation and infrared emission spectral ranges). The collected IR emission was collimated and focused onto a thermoelectrically cooled 2–5 μm mercury–cadmium–zinc–telluride (MCZT) detector (Model PVI-2TE-5, VIGO Systems, Poland) by the parabolic mirror (*PM*2). The signal from the MCZT detector was then sent to the computer for further processing. This set-up has advantages with regard to field measurements in industrial settings compared to other PTR systems reported in the literature: stability and convenience, since there is no liquid-nitrogen-cooled detector; compactness and measurement flexibility through the optical box, which can be easily and independently relocated to inspect diverse case-hardened components; measurement speed, by replacing the expensive bulky hardware-based signal processing instruments associated with conventional point-by-point frequency scans, with a compact high speed data acquisition card and computer-controlled software modules for signal generation and detection.

3. Sample preparation and methodology

Two types of aerospace gear-tooth samples from Avio S.p.A. Torino, Italy, were used in this study. They were made of AISI9310 steel (0.08–0.13% C, 0.45–0.65% Mn, and 0.15–0.3% Si) and Pyrowear53 steel (0.1% C, 1% Si, 2% Ni, 2%Cu, 0.35% Mn, 1% Cr, 3.25% Mo, and 0.1% V). The samples were approx. 25 mm long. The AISI9310 samples were labeled A10, A11, A13, and A_{ref}. The Pyrowear53 samples were labeled P1, P6, P7, and P_{ref}. The subscript "ref" stands for unhardened reference samples. All samples had been subjected to a standard industrial carburizing hardening process, yielding effective case depth variations between 0 and 3 mm for type A (AISI9310) and between 0 and 2.93 mm for type P (Pyrowear53). Effective case depths measured by the conventional destructive Vickers hardness method (HV 0.5) are shown in Table 1. These data were collected by taking measurements at five different sites representative of the major flat and curved surfaces of the (identically shaped) gear teeth, Fig. 2: the inclined surfaces of the V-groove at the top of the gear tooth (Flank 1 and Flank 2); the small-area flat surface of the V-groove crest (Top); the rounded inner bottom surface of the V-groove (Root); the large flat side surface (Flat face). These locations are of major importance for case depth measurements as they are hard to reach with conventional indenters and correspond to critical integrity factors in the design of aerospace parts manufactured with the gear types of this study.

The surface of each sample was cleaned with acetone before measurements to remove contaminants, including oil and finger prints, which might affect the PTR signal. Once cleaned, the sample was put on the sample holder at a fixed angle with respect to the incident laser beam. Our previous studies with these particular steel types [13] indicated that PTR signal features

Table 1
Effective hardened case depths measured by conventional Vickers indenter testing at five sites in six samples (Courtesy: Department of Industrial Technologies, Avio S.p.A., Torino, Italy).

	Effective case depth (*E*)/mm					
	Material	**Flank 1**	**Flank 2**	**Top**	**Root**	**Flat Face**
A10	AISI9310	0.92	0.92	1.11	0.79	0.92
A11	AISI9310	1.01	1.00	1.27	0.9	1.05
A13	AISI9310	1.37	1.4	1.88	1.18	> 3
A_{ref}	AISI9310	unhardened	unhardened	unhardened	unhardened	Unhardened
P1	Pyrowear53	0.84	0.82	1.06	0.51	0.88
P6	Pyrowear53	1.33	1.28	2.00	1.02	1.46
P7	Pyrowear53	1.76	1.72	2.93	1.34	1.89
P_{ref}	Pyrowear53	unhardened	unhardened	unhardened	unhardened	Unhardened

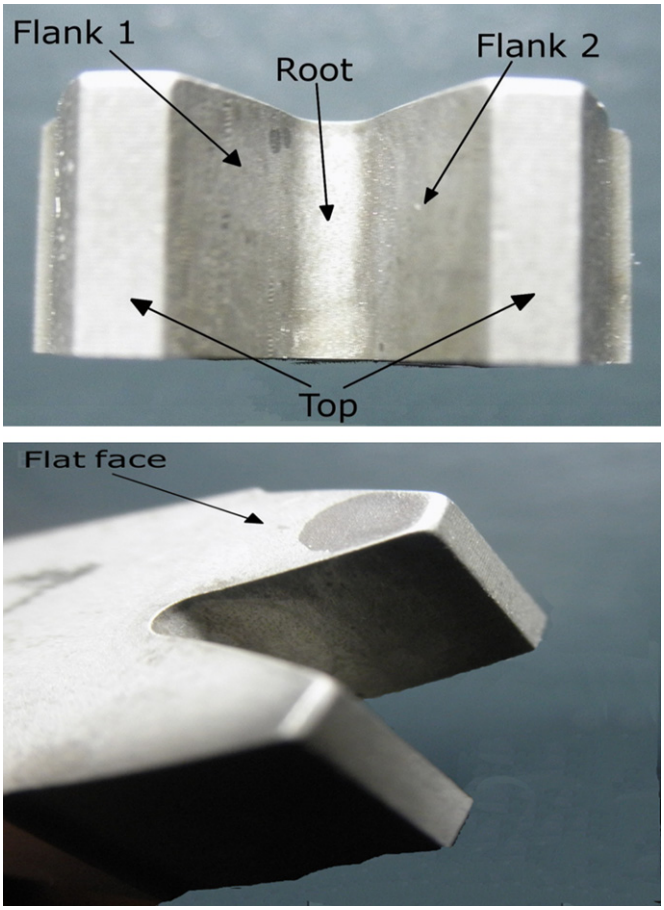

Fig. 2. Topography of gear-tooth samples, indicating the various measurement sites. (a) Top-down view of recessed V-groove; (b) sideways view of flat surface.

specific to hardness case depth are sensitively dependent on the angle of incidence and the concomitant projectional beam shape changes on the surface of steel samples. To maximize reproducibility and optimize SNR, the sample was aligned with the surface perpendicular to the excitation beam (Fig. 1). To minimize edge effects, especially on the limited size areas probed, measurements as far from edges as possible and away from visible inhomogeneities were chosen.

4. The thermal-wave radar (TWR) method

Measurements on the two series of steels (AISI9310, A, and Pyrowear53, P) at five different sites (Flat face, Flank 1, Flank 2, Top, and Root) were carried out using the TWR method. The signal processing scheme is shown below:

$$\xrightarrow{Ref\ Chirp} Y1 = FFT(Ref(x)) \xrightarrow{Y3=(Y2xY1^{*})} Y4 = FFT^{-1}(Y3) \xrightarrow{Y5=Real\ (Y4)} Delay\ time(\tau)$$
$$\xrightarrow{Response\ Chirp\ (PTR)} Y2 = FFT(PTR(x))$$

which corresponds to the cross-correlation integral of the photothermal response to a laser-beam sine-wave modulation with a replica of the excitation modulation waveform (reference) delayed by τ:

$$C(\tau) = \int_{-\infty}^{\infty} f^{*}(t)g(t+\tau)dt \tag{1}$$

Here, the following definitions have been used for numerical cross-correlation computations:

$$Y1 = FFT[\mathrm{Ref}(x)] = Y_k = \sum_{n=0}^{N-1} x_n e^{-j2\pi kn/N} \text{ for } n = 0,1\ldots N-1;$$
$$k = n/2,(n-1)/2 \text{ for } even \text{ and } odd\ n \tag{2a}$$

$$Y2 = FFT[\mathrm{PTR}(x)] = Y_l = \sum_{m=0}^{N-1} x_m e^{-j2\pi lm/N} \text{ for } m = 0,1\ldots N-1;$$
$$l = m/2,(m-1)/2 \text{ for } even \text{ and } odd\ m \tag{2b}$$

$$Y3 = (Y2) \times (Y1^{*}) = Y_k Y_m = \sum_{n=0}^{N-1} x_n \sum_{m=0}^{N-1} x_m e^{-j2\pi(lm-kn)/N} \tag{2c}$$

$$Y4 = X_n = \frac{1}{N}\sum_{k=0}^{N-1} Y_k e^{-j2\pi kn/N} \text{ for } n = 0,1,2,\ldots,N-1 \tag{2d}$$

$$Y5 = X_n = \frac{1}{N}\sum_{k=0}^{N-1} Y_k e^{-j2\pi kn/N} \text{ for } n = even \tag{2e}$$

Starred quantities indicate complex conjugation. In practice, the thermal-wave radar signals were processed as follows: A reference chirp signal in the frequency range of 0.2–2.0 Hz with 10 s duration was generated to modulate the laser. The reference signal and the photothermal response chirp signal from the MCZT detector were acquired through the data acquisition card with the sampling frequency of 51200 Hz. Then the fast Fourier transform (FFT) of the PTR response signal ($Y2$) in chirp form and the FFT complex conjugate of the reference signal ($Y1$) were computed, and both signals were multiplied ($Y3$) to compute the inverse FFT of the effective response signal ($Y4$). Finally the delay time was computed from the peak of the effective response ($Y5$). This procedure was repeated three times to compute the averaged delay time and measurement error at each probing region. Changes in delay time could be related to the coordinate location and were affected by material inhomogeneities.

5. Results and discussion

As long as the thickness of the material layer with poorer thermophysical properties (thermal conductivity and thermal diffusivity) than the substrate in which a thermal wave is launched is commensurate with the thermal wavelength, so that coherent thermal-wave accumulation or depletion conditions at the back interface can contribute to the overall photothermal signal [19], increasing the sample thickness results in increased transport distance for the thermal wave, thus the cross-correlation peak delay time increases [14]. Fig. 3 shows the normalized TWR/cross-correlation output signals for three A samples (A10, A11, and A13) with 0.92 mm, 1.01 mm, and 1.37 mm effective case depths, respectively, obtained with laser incidence on Flank 1, Fig. 2. The cross-correlation curves shown in Fig. 3 are normalized to unity and each one is the mean of three CC measurements. The cross-correlations shown in Fig. 3 are only the data near the peak so as to magnify the small, but statistically significant, time delay variations. The curves are smooth owing to the high density of data sets (2560 data points/CC) and to the high SNR.

Consistent with the foregoing analysis of thermal-wave properties, it can be observed that as the effective case depth increases, cross-correlation peak delay time also increases monotonically. Given that peak delay times are only a function of the thermal-wave transport across the thickness of the hardened layer and do not depend on interfering effects such as surface optical properties, similar to the photothermal phase, the analysis of our data has been based only on cross-correlation peak delay time values.

Fig. 4 shows the cross-correlation peak delay times at three different locations: Flank 1 (4a), Flank 2 (4b) and flat face (4c) for the three hardened and reference samples of type A. The SNR of the reference sample is lower than those of the hardened steels because the surface polish of our reference gears increased the laser beam reflectivity, thereby decreasing the PTR signal. In retrospect, a much better reference solid would have been a fully hardened steel of each type with case depth ~1 cm. Unfortunately, this magnitude of case depth is difficult or impossible to achieve in practice. The delay time does not depend directly on the state of the surface, however, the compromised SNR introduces a large error bar. Behavior similar to Fig. 3 is observed at all

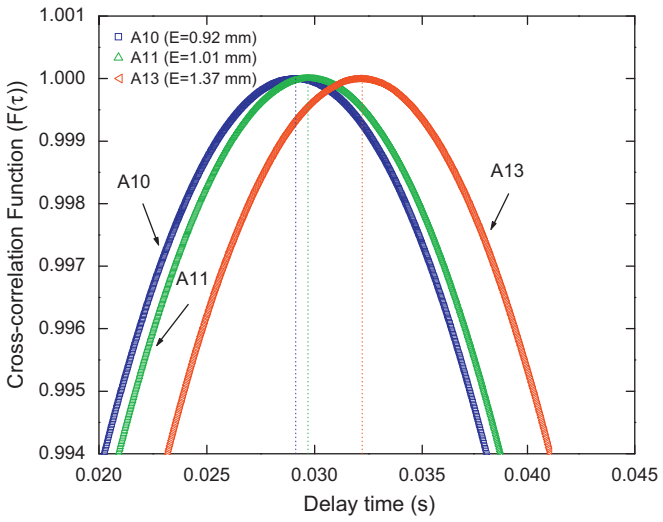

Fig. 3. Experimental normalized cross-correlation function of three A samples (A10, A11, and A13) with different case depths obtained at Flank 1. Chirp bandwidth = 0.2–2.0 Hz, chirp duration = 10 s. The inset shows the case depths as measured with an indenter.

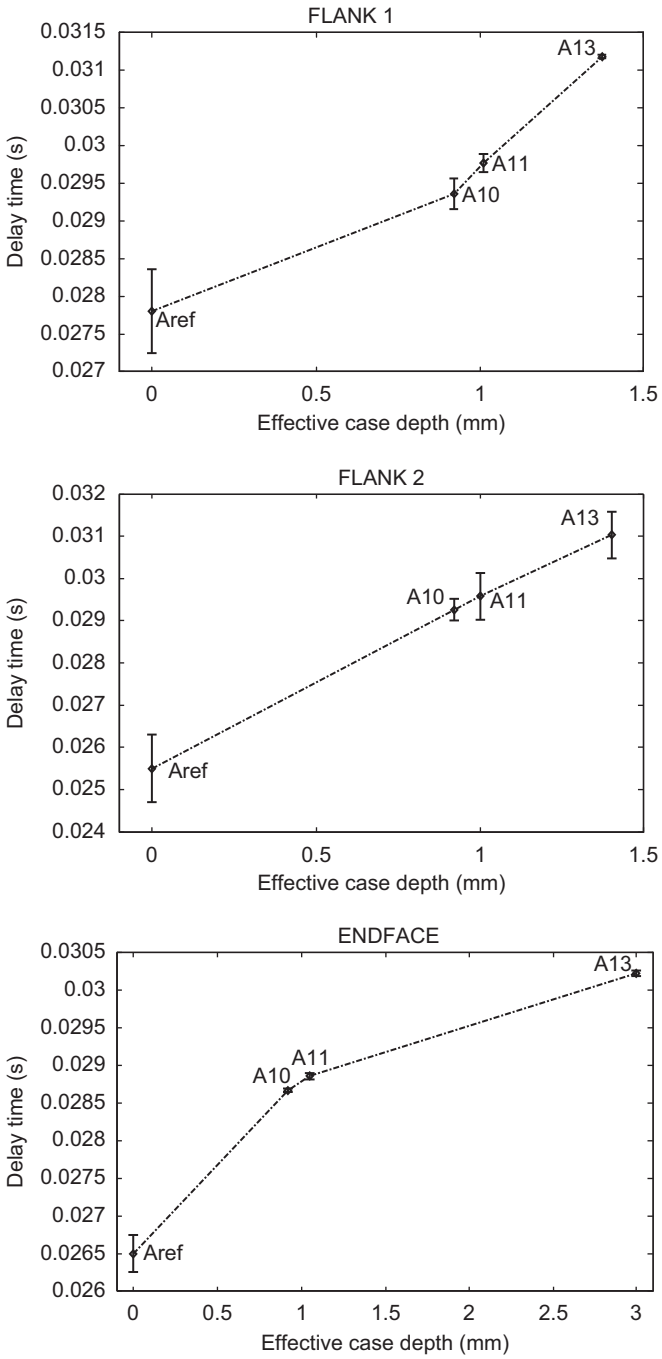

Fig. 4. Cross-correlation peak delay times for type A samples with different effective case depths at three different measurement sites. (a) Flank 1, (b) Flank 2, (c) Flat face. Chirp bandwidth: 0.2–2.0 Hz, chirp duration: 10 s.

three locations, that is, larger effective case depths correspond to longer peak delay time, as expected. The peak delay times associated with the aforementioned three locations and measured on different samples were all very close to each other for a given location. At all these locations the laser beam was positioned far from the edges (> 2 mm), while the maximum thermal diffusion length was on the order of 0.5–1.0 mm. On the other hand, at the remaining sites, Root (Fig. 5a) and Top (Fig. 5b), the peak delay time behavior exhibited greater sample-to-sample variation, while preserving the same delay time increase with increasing case depth. It is possible that these variations were the result of the confined and highly curvilinear geometries of these two locations and the proximity of the laser beam to the edges as

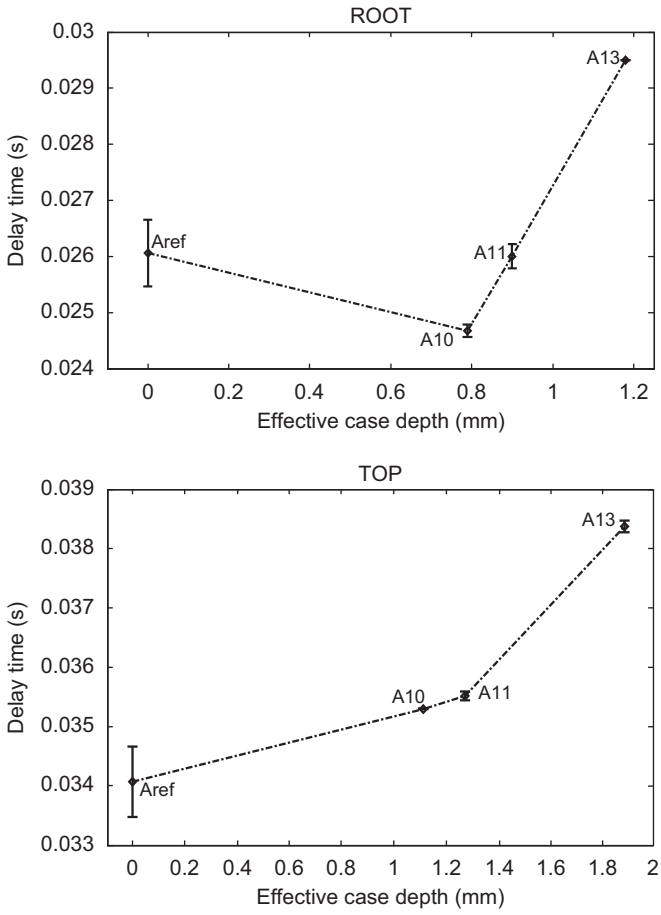

Fig. 5. Cross-correlation peak delay times for type A samples with different effective case depth in two different measurement sites. (a) Top, (b) Root. Chirp bandwidth: 0.2–2.0 Hz, chirp duration: 10 s.

shown in Fig. 2. The observed smaller value of the delay time for the hardened root location compared to the reference sample in Fig. 5 is probably the result of the laser spot not been centered exactly on the root area.

The results of measurements with P steels, Flank 1, Flank 2, and flat face, are shown in Fig. 6. Like the peak delay time relationship with case depth of type A samples, it is clear that here, too, there exists a monotonic correlation. The remaining sites of this series, Top and Root, are shown in Fig. 7 and trends are similar. Overall the P set of samples exhibit better SNR than the A set, primarily because the signal levels were higher.

An overview of the TWR results from both types of samples shows that this PTR method is capable of resolving deeper case depths than the conventional point-by-point and swept-sine frequency scanned PTR. Using AISI9310 samples similar to those utilized in the present study, our earlier tests with swept-sine PTR frequency scans were only able to resolve approx. 1.16 mm maximum case depth [13]; the TWR approach was successful in resolving ca. 3 mm case depths in AISI9310 steels and 1.87 mm in Pyrowear53 steels (Table 1). In the Swept Sine scan method the laser was continuously modulated with sine waves in the frequency range of 1–500 Hz. The corresponding PTR phase response of the various hardened steel samples was measured after the normalization procedure (subtracting the phase of the non-hardened reference sample). Earlier studies using point-by-point PTR frequency scans were only able to resolve ca. 800 μm case depths [7]. The superior performance of the TWR to that of sequential frequency scans in terms of depth resolution has been documented [14] and can be explained through the improvement

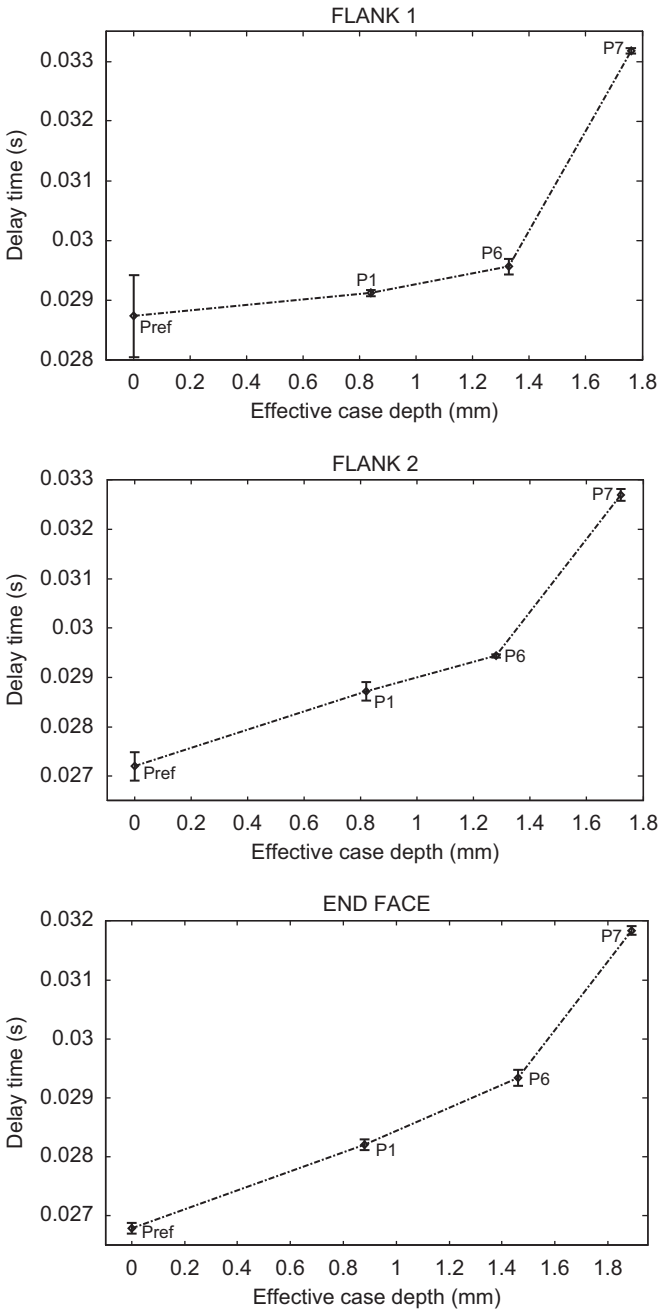

Fig. 6. Cross-correlation peak delay times for type P samples with different effective case depth in three different measurement sites. (a) Flank 1, (b) Flank 2, (c) Flat face. Chirp bandwidth: 0.2–2.0 Hz, chirp duration: 10 s.

of the SNR afforded by the matched filter compression mechanism, which defines SNR as the chirp bandwidth-time product and compresses the photothermal energy into a narrow cross-correlation peak, thereby also enhancing axial resolution.

6. Conclusions

The thermal-wave radar method was used to resolve and measure deep hardness case depths (2–3 mm) of AISI9310 and Pyrowear53 steels used in gears manufactured for the aerospace industry. Monotonic increases of the cross-correlation peak delay time with case depth increases were demonstrated for all samples (several gears) at five locations on the gear: Flank 1, flank 2,

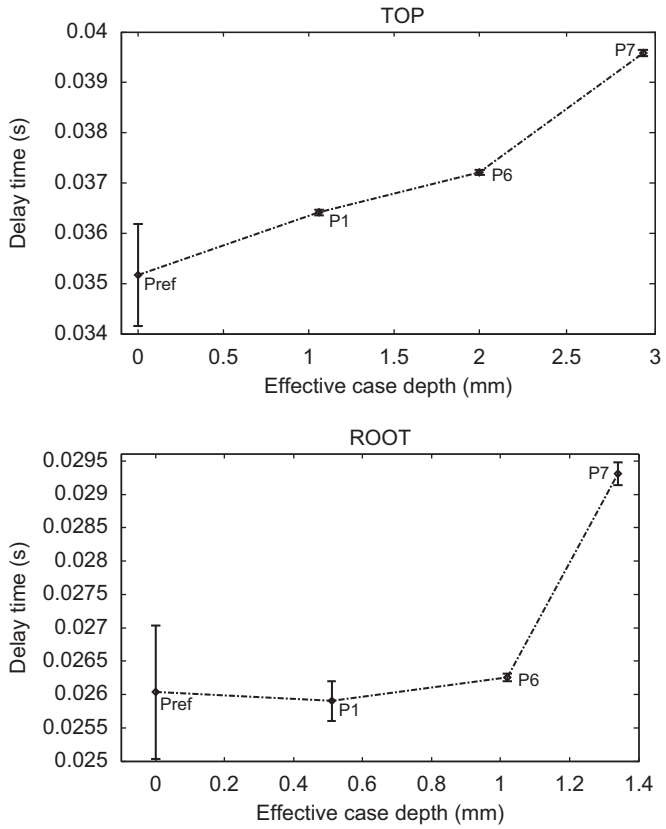

Fig. 7. Cross-correlation peak delay times for type P samples with different effective case depth in two different measurement sites. (a) Top, (b) Root. Chirp bandwidth: 0.2–2.0 Hz, chirp duration: 10 s.

flat face, top, and root. These case depths are the deepest ones measured photothermally to-date, to our best knowledge. The advantages of this method compared to single-frequency PTR and similar broad spectrum photothermal methods are the enhanced SNR of the TWR, which represents the major factor for the improved depth resolution. Additionally, the TWR method leads to significant measurement reduction time.

Acknowledgments

The authors thank to Avio S.P.A. Italy for providing samples. Also, R.V.H. wants to thank CONACYT for financial support that was provided through the project CONACYT 101332 and for a research leave with the CADIFT. A. Mandelis is grateful to the Canada Research Chairs Program.

References

[1] Morgner W, Prietzel KO, Michel F. Non-destructive case depth measuring and monitoring. Proceedings of the XIth international symposium on nondestructive characterization of materials, 2002; 759–765.
[2] Lo CCH, Kinser ER, Melikhov Y, Jiles DC. Magnetic nondestructive characterization of case depth in surface-hardened steel components, In: Review of progress in quantitative nondestructive evaluation 25b, aip conference proceedings. 2006; 820: 1253–1260.
[3] Morgner W, Michel F. Some new results in the field of non-destructive case depth measuring. 9th European NDT Conference (ECNDT2006), Berlin, Germany, September 25-29, 2006.
[4] Honarvar F, Zeighami M. Application of signal processing techniques to case depth measurements by ultrasonic method. Proceedings of the 17th World Conference on Nondestructive Testing. 25-28 Oct. 2008, Shanghai, China, 490.
[5] Zweschper Th, Dillenz A, Scherling D, Busse G. Ultrasonic excited thermography using frequency modulated elastic waves. Insight 2003;45:152–78.
[6] Krapez JC, Li Voti R. Effusivity depth profiling from pulsed radiometry data: comparison of different reconstruction algorithms. Anal. Sci. 2001;17:417–8.
[7] Wang C, Mandelis A. Case depth determination in heat-treated industrial steel products using photothermal radiometric interferometric phase minima. NDT and E Int. 2007;40:158–67.
[8] Munidasa M, Mandelis A. Photothermal imaging and microscopy. Progress in photothermal and photoacoustic science and technology. In: Mandelis A, Ed., vol. 1. New York: Elsevier, 1992.p. 300-358; In: Busse G, Walter HG. Progress in photothermal and photoacoustic science and technology. In: Mandelis A, Ed., vol. 1. New York: Elsevier; 1992. p. 205–298.
[9] Munidasa M, Funak F, Mandelis A. Application of a generalized methodology for quantitative thermal diffusivity depth profile reconstruction in manufactured inhomogeneous steel-based materials. J. Appl. Phys. 1998;83:3495–8.
[10] Depriester M, Hus P, Delenclos S. Sahraoui. New methodology for thermal parameter in solids using photothermal radiometry. Rev Sci. Instrum 2005;76:074902.
[11] Mandelis A, Funak F, Munidasa M. Generalized methodology for thermal diffusivity depth profile reconstruction in semi-infinite and finitely thick inhomogeneous solids. J. Appl. Phys. 1996;80:5570–8.
[12] Qu H, Wang C-H, Guo X, Mandelis A. Reconstruction of depth profiles of thermal conductivity of case hardened steels using a three-dimensional photothermal technique. J. Appl. Phys. 2008;104:113518.
[13] Guo X, Sivagurunathan K, Garcia J, Mandelis A, Giunta S, Milletari S. Laser photothermal radiometric instrumentation for fast in-line industrial steel hardness inspection and case depth measurements. Appl. Opt. 2009;48: C11–23.
[14] Tabatabaei N, Mandelis A. Thermal-wave radar: A novel subsurface imaging modality with extended depth-resolution dynamic range. Rev. Sci. Instrum. 2009;80:034902.
[15] Farnett EC, Stevens GH. Pulse compression radar. In: Skolnik MI, editor. Radar Handbook. New York: McGraw-Hill; 1990. Chap. 10.
[16] Mandelis A. Time-delay-domain and pseudorandom-noise photoacustic and photothermal wave processes: A review of the state of the art. IEEE Trans. Ultrason. Ferroelectr. Freq. Control 1986;UFFC-33:590–614.
[17] Merienne E, Hakem K, Egee M. Photothermal radiometry apparatus using pseudorandom excitation for non-destructive evaluation of layered materials. Mater. Eval. 1994;52:312–6.
[18] Mandelis A, Borm LLM. Frequency modulated (FM) time delay photoacoustic and photothermal wave spectroscopies. Technique, instrumentation, and detection. Part III: Mirage effecte spectrometer, dynamic range, and compatision to pseudo-random-binary-sequence (PRBS) method. Rev. Sci. Instrum. 1986;57:630–5.
[19] Mandelis A, Nicolaides L, Chen Y. Structure and the Reflectionless / Refractionless Nature of Parabolic Diffusion Wave Fields. Phys. Rev. Lett. 2001;87:020801.